

# SONIC BOOM COMPARATIVE STUDY BETWEEN MACH 4.7 OUTDOOR EXPERIMENTAL TESTS AND NUMERICAL SIMULATIONS

Giovanni Fasulo<sup>1</sup>, Luigi Federico<sup>1</sup>, Francesco Petrosino<sup>1</sup>, Samuele Graziani<sup>2</sup>, Nicole Viola<sup>2</sup>, Sebastien Hengy<sup>3</sup>, Bastien Martinez<sup>3</sup> & Marie Albisser<sup>3</sup>

<sup>1</sup>Italian Aerospace Research Centre (CIRA), 81043, Capua, Italy
<sup>2</sup>Mechanical and Aerospace Engineering Department, Politecnico di Torino, 10129, Turin, Italy
<sup>3</sup>French-German research institute of Saint-Louis (ISL), 68300, Saint-Louis, France

#### **Abstract**

This paper presents a comparative analysis of numerical and experimental results from sonic boom tests conducted at ISL's facility as part of the EU-funded H2020 MORE&LESS project. The project's aim is to develop a comprehensive multidisciplinary framework for assessing the environmental impact of supersonic aircraft through multi-fidelity simulations and test campaigns. Therefore, in collaboration with CIRA, ISL conducted a series of outdoor tests, launching a revised configuration of the STRATOFLY MR3 at Mach 4.7 and deploying various type of acoustic sensors to capture sonic boom data. PoliTO's multi-fidelity model utilizes a CFD-based approach to generate detailed near-field signatures based on the aircraft's characteristics. These signatures are then propagated using analytical solutions, providing an efficient means to analyze sonic booms at specified distances with minimal pre-processing requirements.

Keywords: Sonic boom; MORE&LESS; STRATOFLY; CFD; Whitham's modified linear theory.

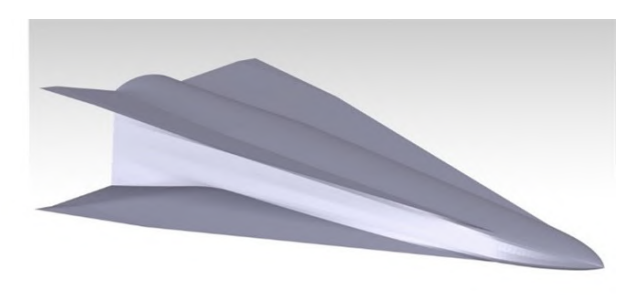
#### 1. Introduction

Recent research indicates that sonic booms can be mitigated to publicly acceptable levels through careful modeling of vehicle geometry [1]. In response, the MORE&LESS project [2] aims to explore the potential of various innovative supersonic aircraft and to develop a comprehensive multidisciplinary framework for assessing their environmental impact through multi-fidelity simulations and test campaigns. While the literature suggests that theoretical models [3, 4, 5] can accurately approximate sonic boom characteristics for most supersonic aircraft [6, 7], these models have inherent limitations, such as the neglect of nonlinear effects in Whitham's formulation [3], which became dominant in the hypersonic regime, and challenges in interpreting the supersonic area-rule concept at high Mach numbers [8]. Therefore, a synergic approach utilizing both low- and high-fidelity models can provide precise outcomes while maintaining the advantage of less pre-processing and computational effort. In this context, a series of outdoor investigation activities were undertaken through collaboration between ISL and CIRA [9]. These activities provided essential experimental data to validate the multifidelity procedures. Specifically, the initial test campaign, conducted at the ISL proving ground approximately 25 km north of Saint-Louis on October  $4^{th}$  and  $5^{th}$ , 2022, focused on a scaled and slightly modified version of the STRATOFLY MR3 vehicle [10]. These models were launched five times using a 91 mm smooth-bore cannon at supersonic speed over a distance of 210 meters, achieving a Mach number of 4.7, with varying projectile initial positions and a zero initial angle of attack. During each test, several meteorological condenser pressure and free-field microphones were deployed on the ground at various distances from the firing line to record the sonic boom. The multi-fidelity approach involves Computational Fluid Dynamics (CFD) simulations to generate detailed near-field signatures based on the geometry and aerodynamic characteristics of the aircraft [11, 12, 13]. These signatures can then be propagated under the assumption that, sufficiently far from the aircraft, they evolve into N-waves. According to this hypothesis, analytical solutions for shock strength and duration [3] are employed to propagate the near-field signatures to the desired distances.

## 2. Experimental Tests Overview

From October 4<sup>th</sup> to 5<sup>th</sup>, 2022, five free-flight tests were conducted on the sub-scale of the STRATOFLY MR3 (Figure 1a) aircraft concept at the ISL's proving ground. Specifically, the model was subjected to both numerical and experimental investigation, including wind-tunnel and shock-tunnel tests. Concurrently, a light redesign was undertaken in order to facilitate launch from a 91 mm smooth-bore powder gun and achieve stability in flight. The proposed modifications, which were implemented to circumvent asymmetric lifting effects during free-flight tests and to preserve the bottom contour, were achieved by mirroring the lower part to the top (no lift generation at zero angle of attack). For simplicity, the canards and fins were not considered. Consequently, the final geometry (Figure 1b) exhibited a mass of 501.7 g and a length of 203 mm, with the center of gravity longitudinally located 132.6 mm from the nose. Moreover, a supportive device was designed to enable a smaller-diameter STRATOFLY model (max. 70 mm) to be fired from the larger-diameter barrel (91 mm). In any case, a sabot package would have been required to prevent gas leakage, ensure stability during flight and the proper transmission of the pressure forces to the projectile mechanical structure. The resulting design consisted of four petals (3D printed) and an aluminum pusher plate.





(a) STRATOFLY MR3 vehicle.

(b) Free-flight STRATOFLY model.

Figure 1 – Proposed geometry modifications for the free-flight tests.

After the gun launch, sabot petals separate from the projectile at a certain distance which depends on both the initial velocity and on the total mass to be fired. To avoid interfering with its trajectory, a sabot catcher and a wood wall were located between 5 and 10 meters from the launcher for catching the sabot petals. Therefore, the models were considered free-flying from a minimum distance – of almost 10 m in the present cases - where no perturbations from the gun or the sabot occur anymore. For illustrative purposes, a representative image of the projectile between the sabot catcher systems, captured by the high-speed cameras, is presented in Figure 2.



Figure 2 – Snapshot of the projectile in flight, close to the sabot catchers.

For each test, the model was launched under atmospheric conditions, over a firing distance of approximately 210 meters, and with rectilinear trajectories. The initial Mach numbers were around 4.7,

and the projectiles were positioned vertically for the initial three tests and in a horizontal configuration for the final two tests (wings parallel to the ground). Table 1 provides a summary of the initial experimental conditions for each shot.

Table 1 – Overview of the test matrix.

Test #	Initial speed $[m/s]$	Initial Mach [-]	Pressure [hPa]	Temperature [°C]	Humidity [%]
1	1616	4.7	995.4	19	69
2	1617	4.7	995.2	20	59
3	1605	4.7	995.7	14	89
4	1609	4.7	995.2	18	72
5	1612	4.7	994.9	23	51

The ISL and CIRA teams deployed a total of 19 ground microphones. Specifically, the measurement setup of ISL consisted of fifteen 1/4-inch Bruel&Kjaer microphones of type 4938, positioned at a 30 centimeter height from the ground, at five different CPA (Closest Point of Approach) distances of 5, 10, 15, 20, and 30 meters on three lines at distances of 70, 85, and 100 meters from the canon muzzle (Mic1 to Mic15 of Figure 3). CIRA extended the measurement setup by adding four 1/4-inch PCB 377A12 microphones (Ch1 to Ch4 of Figure 3) at a height of one meter and at distances of approximately 5 and 10 meters from the trajectory. The data acquisition and storage were handled with a data recorder from the TEAC Corp. with a sampling frequency of 192 kHz (for ISL ground acoustic equipment) and with an 8-channel real-time sound level integrator and analyzer, from the Imc Corp., at a sampling rate of 51.2 kHz per channel (CIRA). In all cases, the starting and ending phases of signals acquisition were performed manually during the countdown process preceding the recorded shot and once the shot was triggered.

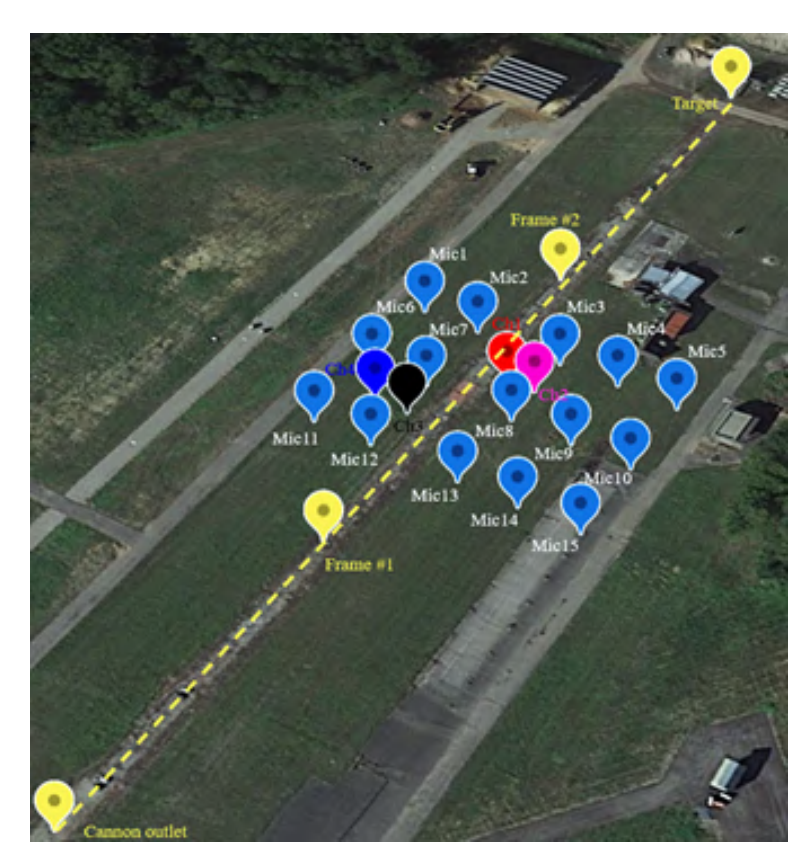


Figure 3 – Position of ISL and CIRA ground microphones, roll angle detection frames, cannon outlet and target.

#### 2.1 CPA Estimation

In order to compare the experimental and numerical results, it was essential to compute the geometric relationship between the microphone sensors and the model in flight for each shot. This also includes the estimation of the Closest Point of Approach (CPA), namely the minimum distance between the firing line (cannon exit and exit frame positions, i.e., the yellow line in Figure 3) and the acoustic sensors. Consequently, the Haversine formula was employed to calculate the great-circle distance between two points on a sphere, and the cosine formula was utilized to estimate both parallel and perpendicular distances from the trajectory of each microphone. In particular, the CPA of each ground acoustic sensors are gathered in Table 2:

Table 2 – ISL and CIRA estimated CPA for each ground microphone.

Label	CPA [m]	
Mic1	14.7	
Mic2	4.9	
Mic3	10.4	
Mic4	20.3	
Mic5	30.3	
Mic6	14.8	
Mic7	5.0	
Mic8	10.3	
Mic9	20.4	
Mic10	30.2	
Mic11	15.0	
Mic12	5.0	
Mic13	10.2	
Mic14	20.1	
Mic15	30.1	
Ch1	5.4	
Ch2	10.1	
Ch3	4.2	
Ch4	9.9	

#### 2.2 Roll Angles Estimation

The non-axisymmetric nature of the projectile influences the spatial distribution of sonic booms, with the resulting sound field varying according to the model's roll angle. Therefore, accurately estimating these angles is crucial in producing reliable and valid comparisons between experimental observations and numerical simulations. Given the difficulty of obtaining precise measurements of the roll angles associated with microphone recordings of sonic booms, a reasonable approximation has been introduced in this study. Specifically, as the shock wave system generated by the supersonic projectile expands outward at the speed of sound along the  $\overline{BC'}$  direction, the sound measured at position C' was considered to be related to the roll angle at the detach point B of the shock wave (Figure 4).

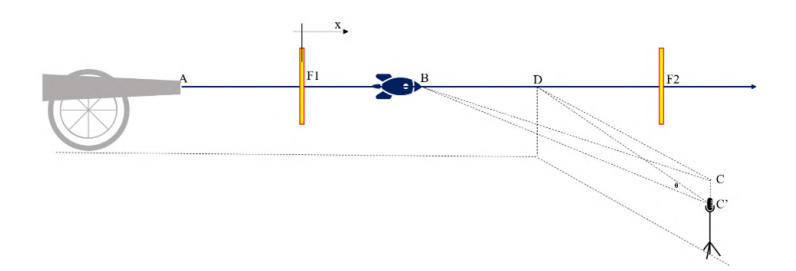


Figure 4 – Representation of the positioning of roll angle detection targets and of the shock wave path considered for roll angle estimation.

Specifically, the procedure to estimate the evolution of the roll angle involved installing two paper frames (Figure 5) at the entrance and exit of the acoustic measurement zone (F1 and F2 in Figure 4).



Figure 5 – Paper frames at the entrance and exit of the acoustic measurement zone.

Table 3 provides a summary of roll angle measurements taken at both stations for each shot. It should be noted that all roll angles are defined in relation to the vertical upward direction.

Table 3 – Roll angle r	measurements	for	each	test.
------------------------	--------------	-----	------	-------

Test #	Roll angle frame 1 $arphi_1$ [deg]	Roll angle frame 2 $\varphi_2$ [deg]	Direction of rotation
1	0.5	18.6	Anticlockwise
2	39.8	63.1	Anticlockwise
3	122.0	141.8	Anticlockwise
4	-39.5	-50.6	Clockwise
5	9.5	3.5	Clockwise

These two local information were generalized by assuming a constant angular velocity within the acoustic measurement zone, enabling the use of linear interpolation of Eq. (1). To estimate the effective roll angle for each test and microphone, the x coordinate was set equal to the difference between the distance  $\overline{AB}$  and the distance from the cannon outlet to the first paper frame  $(\overline{AF_1})$ . The value of  $\overline{AB}$  can be calculated using a geometric acoustic model [9], while the value of  $\overline{AF_1}$  remains constant for each test and is equal to 52.4 m.

$$\varphi(x) = \frac{\varphi_2 - \varphi_1}{\overline{F_1}\overline{F_2}}x + \varphi_1 \tag{1}$$

At this stage, an adjustment in roll angle becomes indispensable. As illustrated in Figure 6, a roll angle of zero degrees, referenced from the default coordinate system (indicated by yellow), does not signify a perfectly horizontal alignment concerning the probes; rather, it indicates a slightly different one. The adjustment process involved the utilization of two distinct local coordinate systems. The objective was to align the roll angle to zero when the model assumes a horizontal orientation (ontrack) relative to the acoustic sensor and to 90 degrees when the model is vertically aligned with the probe. These new local coordinate systems were derived by adding (blue coordinate system) or subtracting (green coordinate system) the angles between the horizontal line and the line connecting the fire trajectory to the probes from the roll angle  $\varphi$ , measured from the vertical upward direction. The decision to add or subtract was contingent upon the relative positioning of the probes in relation to the shot trajectory, as delineated in Figure 6 (left or right).

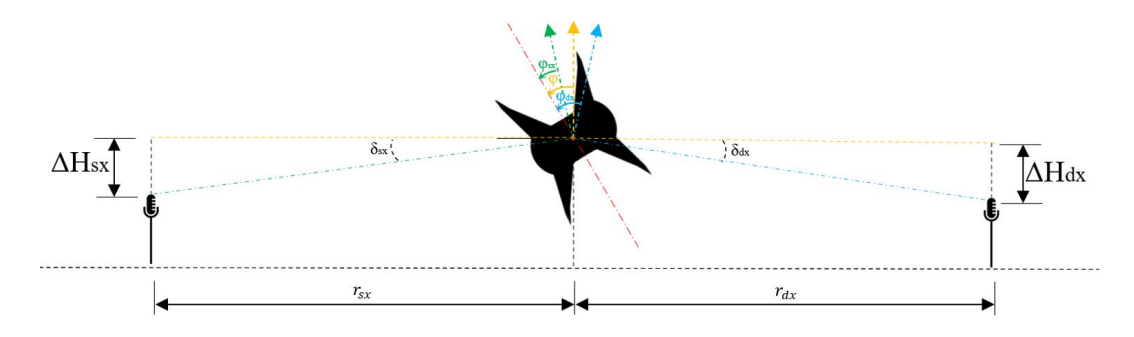


Figure 6 – Front view of the first three test setup.

As previously discussed, projectiles roll angles were calculated for each microphone position in the field and for each shot. The results are presented in Table 4.

Table 4 – ISL and CIRA estimated roll angles for each shot [degrees].

Label	Test #1	Test #2	Test #3	Test #4	Test #5
Mic1	18.7	61.6	38.6	41.4	11.1
Mic2	30.2	73.3	27.1	30.7	21.9
Mic3	4.6	47.6	52.7	55.8	3.2
Mic4	8.3	51.2	49.0	51.2	1.2
Mic5	9.2	51.8	48.2	49.4	2.8
Mic6	14.7	56.6	42.9	39.0	12.4
Mic7	26.3	68.3	31.3	28.4	23.2
Mic8	0.8	42.6	56.9	53.4	1.9
Mic9	4.4	46.1	53.3	48.8	2.5
Mic10	5.3	46.9	52.4	47.0	4.1
Mic11	10.9	51.5	47.2	36.6	13.7
Mic12	22.4	63.3	35.6	26.0	24.5
Mic13	3.1	37.6	61.1	51.0	0.7
Mic14	0.5	41.2	57.5	46.4	3.8
Mic15	1.4	41.9	56.7	44.7	5.4
Ch1	5.2	47.7	52.3	52.6	0.5
Ch2	8.0	50.5	49.4	49.6	2.5
Ch3	17.6	59.1	40.1	34.6	16.6
Ch4	12.4	53.9	45.4	39.3	11.7

### 3. Numerical Investigation

To validate the results obtained during the experimental test, a numerical investigation of the case study has been performed. In particular, computational fluid dynamics (CFD) is usually employed to study the flow around a supersonic aircraft due to the strong non linearities and three dimensional interactions. In the proximity of the configuration, the aerodynamic effects are more relevant compared to the refraction effects of an inhomogeneous atmosphere, which would gain more importance in the subsequent far-field propagation of the sonic boom. Over the last two decades, sonic boom prediction has undergone to numerous improvements, and NASA, since 2014 has proposed the AIAA Sonic Boom workshop [11] [12] [13] which had the aim to investigate the best numerical methodology to estimate sonic boom for both generation and propagation. The cross-validated methodologies and results of the three workshop's participants represent the state-of-the-art in the prediction in the near field region of a supersonic object.

In this work it was used the commercial software ANSYS-Fluent [14], that employ an unstructured finite-volume approach to solve the Reynolds-Averaged Navier-Stokes (RANS) equations, with gradients computed using a Green-Gauss method and an adaptive CFL is employed as a convergence

strategy. The simulations are carried out without considering a turbulence model, solving inviscid Euler equations with an ideal gas model for the air. Previous work highlight the possibility of correctly investigate shock waves produced by a supersonic aircraft by solving Euler equations without losing of accuracy.

The definition of the mesh, in terms of refinements and adaptation approach allows to proper tracking of discontinuity needs specific effort. The grid is composed by two different parts: a cylindrical unstructured grid in the vicinity of the aircraft and a structured grid created with a blocking technique far from the geometry aligned with the Mach angle  $\mu$  as could be seen in Figure 7 and 8. The numerical elements are hexahedral in the structured part, tetrahedral in the unstructured zone, and pyramids to connect the two zones. Within this approach, the total number of elements are about 30 millions, and it can provide accurate estimation of noise.

Compared with a full unstructured or full structured mesh approach, the mixed-grid strategy has the advantage to preserve accuracy as well as efficiency.

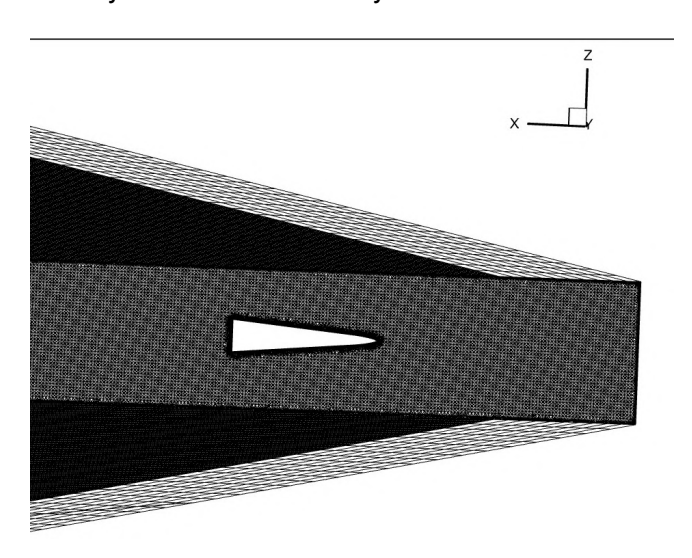


Figure 7 – Hybrid Grid Approach.

Previous research [15] has pointed out the importance of maintaining good alignment in the grid. Specifically, for high displacement in the z direction, differences in the signature for slightly misaligned grids were noticeable. Moreover, Cartesian meshes can be effective for out-of-body signature computation as long as the mesh is nearly aligned with the Mach angle  $\mu$ . Good alignment reduces dissipative effects and the number of elements, enabling signatures to be computed for distances up to H/L=5 without incurring extremely high computational costs. The H/L ratio represents the distance of extraction relative to the body length of the aircraft; for instance, H/L=3 corresponds to a distance of extraction of three body lengths below the aircraft, and for this case study is about 61 cm below the configuration.

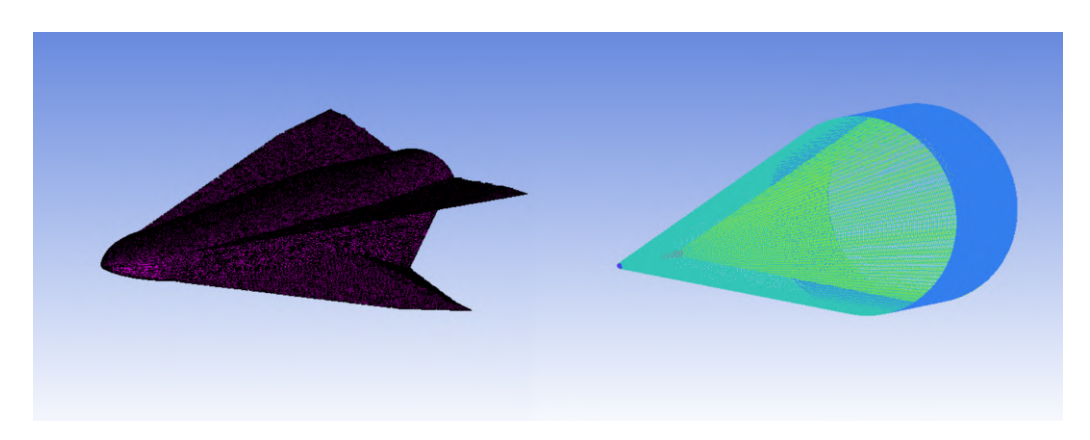


Figure 8 – Detail of the domain and MR3 STRATOFLY.

As a numerical scheme adopted for these simulations, advection upstream splitting method (AUSM) was employed. The scheme's rely in breaking the flux vector into both the convective and pressure components, and allows AUSM to accurately captures shock discontinuities without introducing numerical artifacts. The use of an upwinding strategy allows the methods to calculate the fluxes at cell interfaces, ensuring accurate information transfer across the computational domain. Also, AUSM employ unfixed flux-splitting coefficients and they can dynamically adjusts based on local flow conditions, guaranteeing stability and accuracy across various flow regimes. Additionally, it incorporates a flux-difference splitting approach, improving accuracy near discontinuities by considering both convective and pressure-gradient terms comprehensively. Previous works related to sonic boom adopted AUSM numerical scheme to correctly evaluate the shock waves generation with different supersonic configurations [16] [17] [18].

Noise performances evaluation of MR3 STRATOFLY aircraft, in the operating conditions of the tests shows the capability of the computational approach explained in the previous paragraphs. The pressure variation in the aeroacoustic problems is usually evaluated with the formulation:

$$\Delta p/p = \frac{p_s - p_0}{p_0} \tag{2}$$

In Equation (2)  $p_0$  is the free-stream static pressure and  $p_s$  is the one extracted at a specific height to length H/L location.

The shock waves around the MR3 STRATOFLY aircraft are clearly visible in Figure 9. Due to the symmetry of the configuration, as expected the aerodynamic field between the upper and lower part of the configuration is the same.

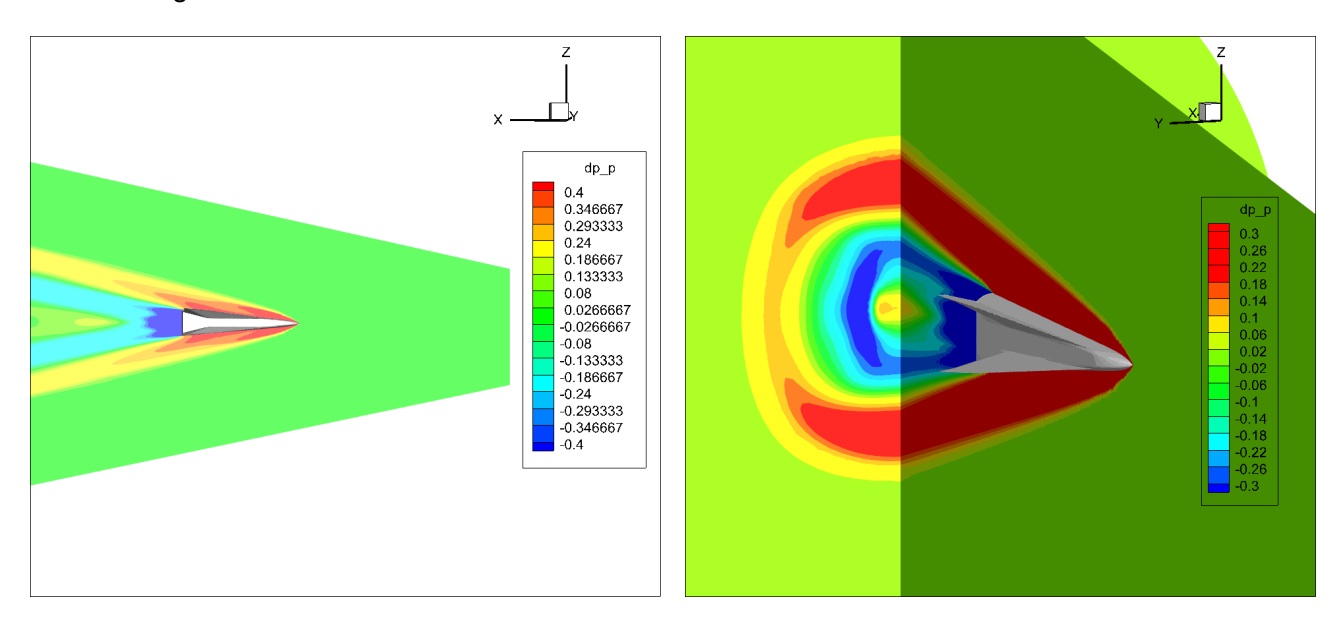


Figure 9 – Contours of the MR3 simulations.

The pressure signatures were extracted at H/L=3 and H/L=5 for the configuration as they are visible in Figure 10.

The typical N-wave shape of the pressure variation is well simulated, with a good definition. As highlighted in the contours of Figure 9, the radial evaluation of delta pressure is different between the on-track and off-track condition, and it is validated by the extracted pressure signatures.

The condition with the highest value of noise is the one below the aircraft, and the shape of the pressure signatures does not vary with different angle of extractions. Finally, the difference between the peak pressure in the overpressure domain and the one of expansion part is almost negligible.

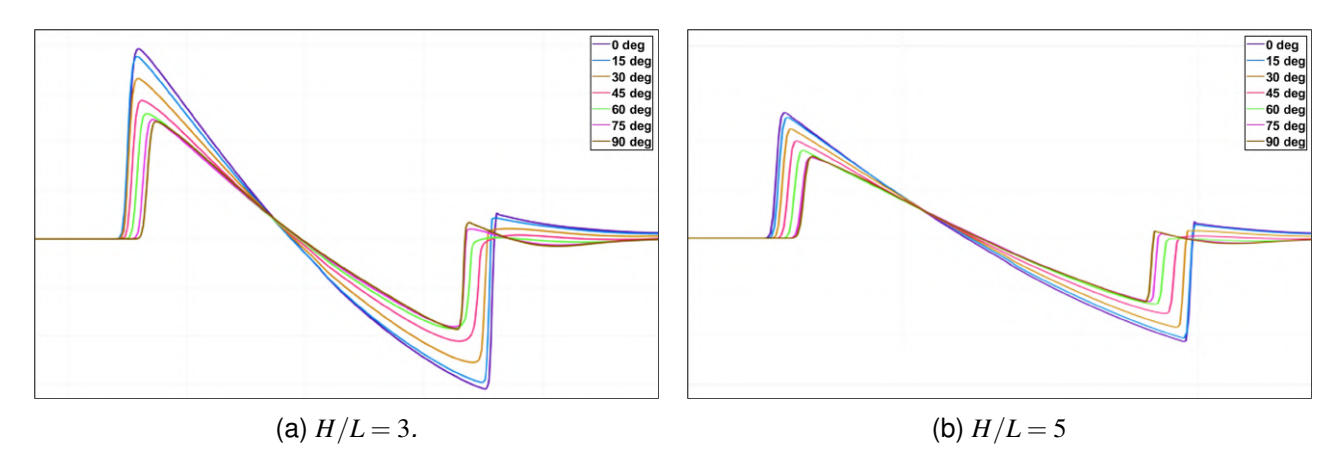


Figure 10 – Pressure signatures.

#### 4. Results

In the context of this work, a straightforward procedure was implemented to ensure the comparability of numerical and experimental data. The numerical signatures were measured at distances from the body of up to five times the length of the model (approximately 1 m). However, in order to align such results with experimental measurements, the simulated signatures must be propagated to the distances corresponding to the microphone placements in the experimental setup. The simulated signatures were assumed to satisfy the far-field conditions (N-wave shape). Consequently, appropriate scaling could be applied in accordance with Whitham's divergence law [3]:

$$\Delta p \propto r^{-3/4} \tag{3}$$

$$\Delta t \propto r^{1/4} \tag{4}$$

It is important to note that this acoustic divergence law is valid under the assumption of a homogeneous atmosphere (reasonable assumption given the distances between the microphones and the trajectories in comparison to the model dimensions). The procedure began with constructing a fictitious N-wave (Figure 11), derived by considering the peak pressure of the positive phase from the CFD near-field pressure signatures. The duration of the N-wave was instead defined as the time interval between the compression and expansion peaks. Since the numerical extractions were conducted at a location sufficiently distant to ensure far-field conditions, the resulting interpolated N-waves preserved the essential characteristics observed in the simulated signatures.

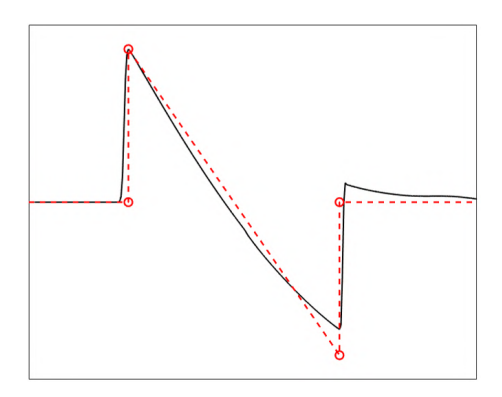


Figure 11 – N-wave approximation (red dotted line) of the simulated signature at 0° roll angle (black solid line).

Figure 12 to 13 present a comparison between the calculated and experimental results for the tests listed in Table 1. The CPA distances in Table 2 were approximated to integer values, resulting in five groups of measurements (5, 10, 15, 20, and 30 meters from the trajectory). For each group, nineteen simulated signatures (one every five degrees) were propagated using the aforementioned procedure

and subsequently interpolated. The experimental data for each CPA group were correlated with the roll angles reported in Table 4. Specifically, Figure 12 and Figure 13 illustrate the duration and peak pressure level values of the N-waves, respectively, as functions of roll angle. The results are reported in the 0-90° range due to the projectile's double symmetry. Overall, there is a quite good alignment between the experimental observations and the CFD results, particularly for both peak pressure levels and durations across track angles up to 40 degrees. However, a greatest disparities between the experimental and CFD values occur within the 40-90 degrees range. Specifically, the shock peak pressure levels predicted tend to be lower than those observed in the experiments. Although the predicted duration shows a similar trend, it exhibits considerable fluctuations within the intermediate roll angles range. This variability may be attributed to various factors, such as the rapid angular acceleration of the projectile and the inability to maintain a constant rotational speed in the acoustic measurement zone.

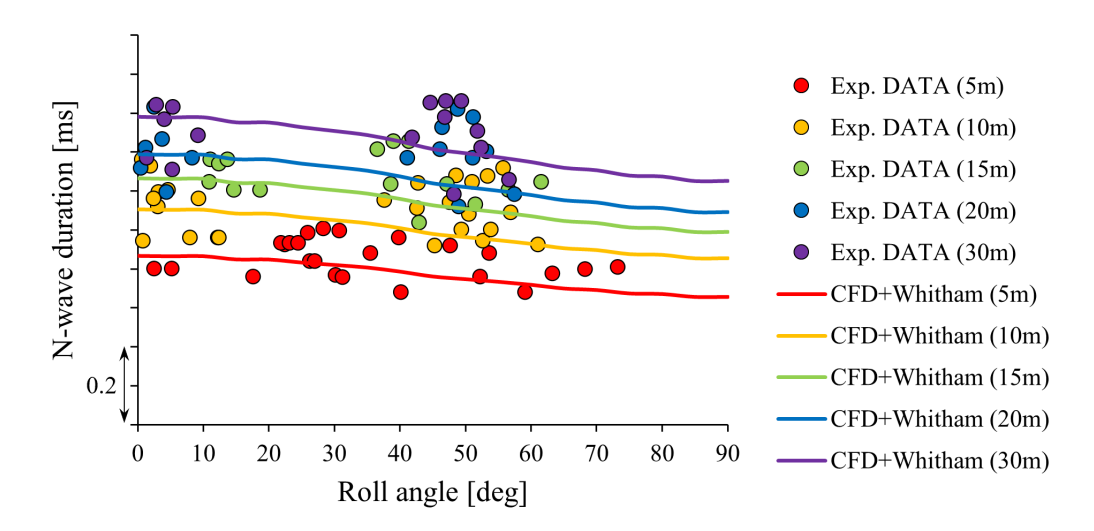


Figure 12 – Comparison of experimental and numerical N-waves duration.

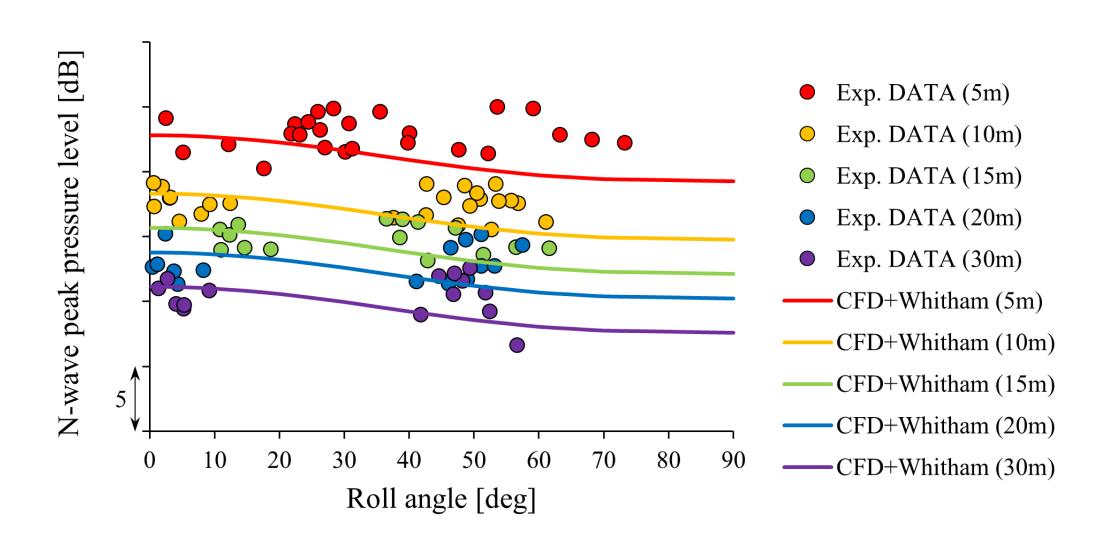


Figure 13 - Comparison of experimental and numerical N-waves peak pressure level.

Due to the rolling motion and the non-axial symmetry of the model, the shock wave fronts form a time-dependent wave envelope. Consequently, as long as the roll rate is minimal and there is no acceleration, experimental results can be reliably compared with numerical results (the latter obtained from a static simulation). However, it is very difficult to fulfill these strict constraints. Therefore, it is more practical to consider average values. Furthermore, this approach allows the comparison of predicted and experimental results as a function of distance from the trajectory, effectively neglecting the

model noise directivity. The following procedure was adopted to calculate the mean pressure values. Specifically, to effectively capture the energy content of the waves, it was computed the mean value of the acoustic pressure from the squares of the pressure peaks. First, peak pressure measurements were collected over the recorded roll angles and for each fixed Closest Point of Approach (CPA). For each pressure peak, the square was computed. These values were then summed for each CPA and divided by the number of measurements. Finally, the square root was taken to determine the mean acoustic pressure value. With regard to the duration, a straightforward mean of the N-wave time duration was considered over the recorded roll angles and for each fixed CPA. The computation of the mean values from numerical predictions follows an identical procedure. However, a pre-processing step was necessary. Indeed, to enable a correct comparison of results, it is essential that the numerical pressure and duration values correspond to the same experimental roll angle range, rather than the entire 0 to 90-degree roll range. Consequently, for each CPA, the numerical results were linearly interpolated to match the experimental roll angles. Subsequently, the aforementioned procedure was employed to process these values (for each experimental roll angle and CPA).

Figure 14 and Figure 15 present both the predicted and measured N-waves in terms of mean peak pressure level and mean duration as a function of the distance from the flight trajectory (CPA).

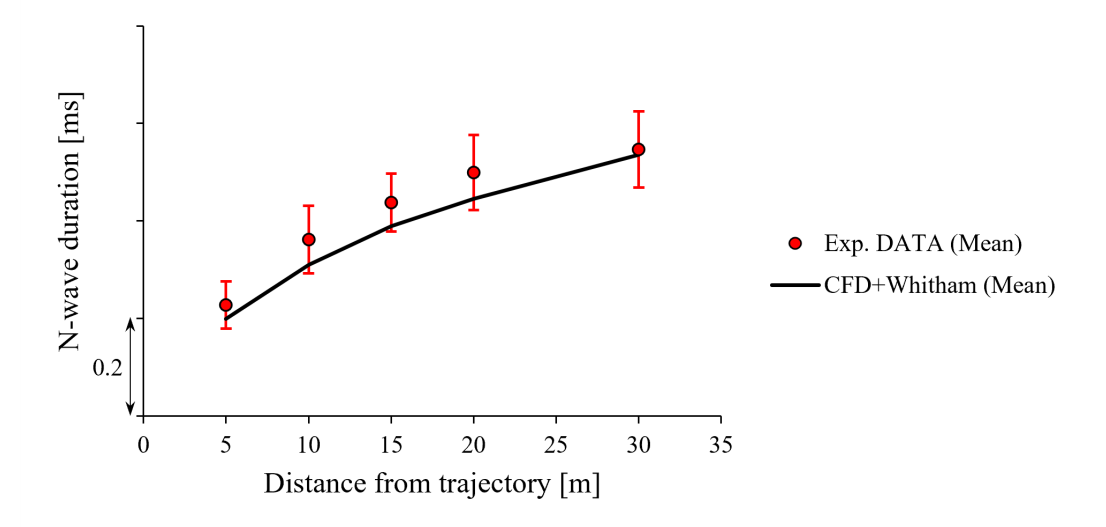


Figure 14 – Comparison of experimental and numerical N-waves duration.

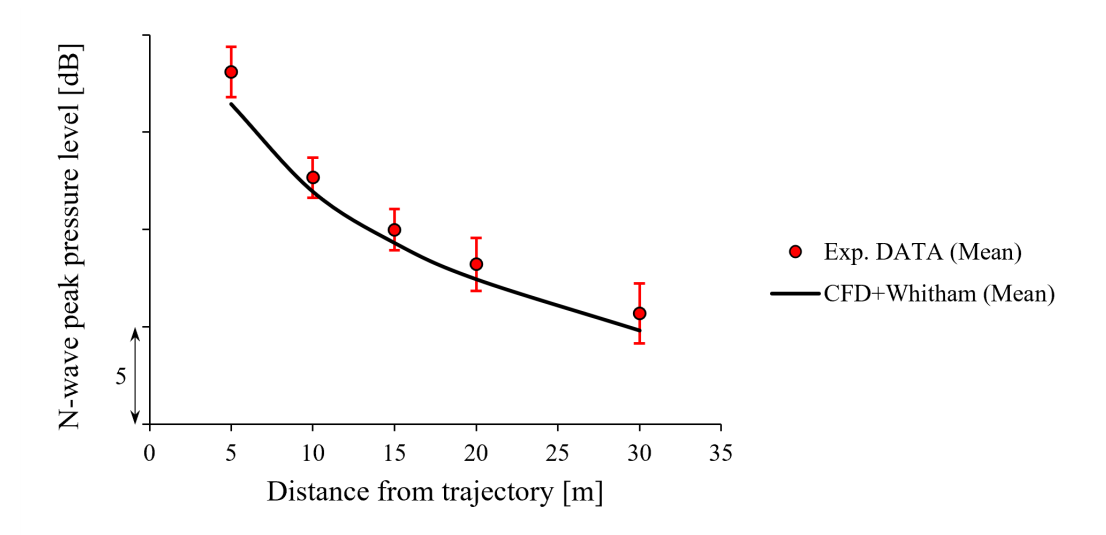


Figure 15 – Comparison of experimental and numerical N-waves peak pressure level.

The scatter plots show the measured values, while the solid line shows the predicted behavior. In or-

der to better interpret the reliability and consistency of the data, error bars were included. Specifically, these represent the standard deviation of measurements.

The graphs suggest that the numerical procedure employed, despite the use of the simplified Whitham propagation law, successfully predicted the essential features (mean behavior across the roll angles) of the sonic boom generated by the STRATOFLY scaled model. Specifically, the peak pressure level estimation presents a mean absolute error of 0.9 dB and a standard deviation of 0.4 dB. The mean error and standard deviation for N-wave duration estimation are 0.039 ms and 0.019 ms, respectively.

#### 5. Conclusions

As part of the EU-funded H2020 MORE&LESS project, an outdoor sonic boom test campaign was conducted at the ISL test ground in Saint-Louis, France. The experimental activity took place over two days, October 4 and 5, 2022, using a scaled and slightly modified version of the STRATOFLY MR3 vehicle, which was launched from a 91 mm smooth-bore powder cannon at an initial Mach number of 4.7. Sonic boom measurements were collected at various points along the range using 19 metrological condenser microphones deployed by ISL and CIRA.

The experimental sonic boom pressure signatures acquired during the test campaign provided essential validation data for the multi-fidelity approach used to predict the sonic boom of the STRATOFLY model. This approach integrates CFD simulations to generate detailed near-field signatures based on the aircraft's geometry and aerodynamic characteristics. These signatures were subsequently propagated to the desired distances using Whitham's analytical solutions for shock strength and duration in the far-field. Specifically, the paper reports the procedure to effectively capture shock waves from a supersonic projectile using a commercial software.

The recorded signals were gathered and post-processed to evaluate the combined effects of roll motion - resulting from manufacturing model uncertainties and varying initial roll positions - and the model's non-axisymmetry on the measured overpressure signatures. There was a quite good alignment between the predicted and observed values for both peak pressure levels and durations across the roll angles up to 40 degrees. However, significant discrepancies emerged within the 40-90 degrees range, where the predicted shock peak pressure levels tend to be lower than those observed experimentally. Although the experimental durations showed a trend similar to the predicted values. they exhibited considerable fluctuations within the intermediate roll angles range. This variability may be attributed to factors such as the rapid angular acceleration of the projectile and the inability to maintain a constant rotational speed in the acoustic measurement zone. Consequently, it was deemed more practical to consider average values. This approach enabled the comparison of predicted and experimental results as a function of distance from the trajectory, effectively neglecting the model noise directivity. Overall, the comparison indicated that the multi-fidelity procedure employed, despite utilizing the simplified Whitham propagation law, successfully predicted the essential features (mean behavior across the roll angles) of the sonic boom generated by the STRATOFLY model. Specifically, the results demonstrated reliability with a mean absolute error of 0.9 dB for peak pressure levels and a standard deviation of 0.4 dB. For the N-wave duration estimation, the mean error was 0.039 ms with a standard deviation of 0.019 ms.

# 6. Contact Author Email Address

mailto: g.fasulo@cira.it

## 7. Copyright Statement

The authors confirm that they, and/or their company or organization, hold copyright on all of the original material included in this paper. The authors also confirm that they have obtained permission, from the copyright holder of any third party material included in this paper, to publish it as part of their paper. The authors confirm that they give permission, or have obtained permission from the copyright holder of this paper, for the publication and distribution of this paper as part of the ICAS proceedings or as individual off-prints from the proceedings.

# References

[1] Ordaz, I., Wintzer, M., Rallabhandi, S. K.: Full-carpet design of a low-boom demonstrator concept. In 33rd AIAA Applied Aerodynamics Conference. (2015)

- [2] Project-MORE&LESS. https://cordis.europa.eu/project/id/101006856 (2020). Accessed 1 January 2024
- [3] Ritzel, D. V., Gottlieb, J. J.: The overpressure signature from a supersonic projectile. UTIAS Report, No. 279 (1987)
- [4] Whitham, G. B: The flow pattern of a supersonic projectile. Communications on pure and applied mathematics, 5(3), 301-348 (1952)
- [5] Walkden, F.: The shock pattern of a wing-body combination, far from the flight path. Aeronautical quarterly, 9(2), 164-194 (1958)
- [6] Maglieri, D. J., Bobbitt, P. J., Plotkin, K. J., Shepherd, K. P., Coen, P. G., Richwine, D. M.: Sonic boom: Six decades of research. (2014)
- [7] Carlson, Harry W. Simplified sonic-boom prediction. (1978)
- [8] Carlson, H. W., Mack, R. J.: A wind-tunnel study of the applicability of far-field sonic-boom theory to the space shuttle orbiter. (1978)
- [9] Fasulo, G., Hengy, S., Martinez, B., Federico, L., De Vivo, L., Albisser, M., Zeiner, A. Experimental Outdoor Activity on Sonic Boom Assessment of the STRATOFLY MR3 Scale Model. Proceedings of HiSST. (2024)
- [10] Viola, N., Fusaro, R.A., Saracoglu, B.H., Schram, C., Grewe, V., Martínez, J.A., Marini, M., Hernández, S., Lammers, K., Vincent, A., Hauglustaine, D., Liebhardt, B., Linke, F., & Fureby, C.: Main challenges and goals of the H2020 STRATOFLY project. Aerotec. Missili Spaz. (2021). https://doi.org/10.1007/s42496-021-00082-6
- [11] Park, M.; Morgenstern, J. Summary and Statistical Analysis of the First AIAA Sonic Boom Prediction Workshop. 2014, Vol. 53. https://doi.org/10.2514/6.2014-2006.
- [12] Park, M.A.; Nemec, M. Nearfield Summary and Statistical Analysis of the Second AIAA Sonic Boom Prediction Workshop. *Journal of Aircraft* 2019, 56, 851–875. https://doi.org/10.2514/1.C034866.
- [13] Park, M.A.; Carter, M.B. Nearfield Summary and Analysis of the Third AIAA Sonic Boom Prediction Workshop C608 Low Boom Demonstrator 2021. https://doi.org/10.2514/6.2021-0345.
- [14] Ansys Fluent Fluid Simulation Software; ANSYS, Inc., 2018
- [15] Park, M.A.; Campbell, R.L.; Elmiligui, A.A.; Cliff, S.E.; Nayani, S., Specialized CFD Grid Generation Methods for Near-Field 555 Sonic Boom Prediction. In 52nd Aerospace Sciences Meeting. https://doi.org/10.2514/6.2014-0115
- [16] Dagrau, F.; Loseille, A.; Din, I.S.E., Computational and Experimental Assessment of Models for the First AIAA Sonic Boom Prediction Workshop Using Adaptive High Fidelity CFD methods. *In 32nd AIAA Applied Aerodynamics Conference*. https://doi.org/10.2514/6.2014-2009.
- [17] Yamashita, R.; Suzuki, K., Full-Field Sonic Boom Simulation in Real Atmosphere. *In 32nd AIAA Applied Aerodynamics Conference*. https://doi.org/10.2514/6.2014-2269.
- [18] Luquet, D.; Marchiano, R.; Coulouvrat, F.; Din, I.S.E.; Loseille, A., Sonic Boom Assessment of a Hyper-sonic Transport Vehicle with Advanced Numerical Methods. *In 21st AIAA/CEAS Aeroacoustics Conference*. https://doi.org/10.2514/6.2015-2685.